Static quark potential from center vortices in the presence of dynamical fermions

James C. Biddle, Waseem Kamleh, and Derek B. Leinweber
Centre for the Subatomic Structure of Matter, Department of Physics, The University of Adelaide, South Australia 5005, Australia

(Received 2 June 2022; accepted 30 August 2022; published 12 September 2022)

For the first time, center vortices are identified on SU(3) lattice ensembles that include dynamical fermions. Using a variational method, the static quark potential is calculated on untouched, vortex-removed, and vortex-only fields. Two dynamical ensembles and one pure gauge ensemble are studied, allowing for an exploration of the impact of dynamical fermions on the center-vortex vacuum. Novel modifications to the standard Coulomb term are introduced to describe the long range behavior of the vortex-removed potential. These modifications remove a source of systematic error in the fitted string tension on the original ensembles. Our pure Yang-Mills result is consistent with previous studies, where projected center-vortex fields only reproduce approximately two thirds of the string tension. Remarkably, we find that the vortex-only fields on both dynamical lattices are able to fully reproduce the respective untouched string tensions.

DOI: 10.1103/PhysRevD.106.054505

I. INTRODUCTION

Over recent years, center vortices have been shown to play a pivotal role in the generation of dynamical chiral symmetry breaking and quark confinement in the QCD vacuum [1–28]. In pure-gauge QCD, it has been shown that vortex removal results in a loss of dynamical mass generation [22,24,26], loss of string tension [21,29] and the suppression of the infrared Landau gauge gluon propagator [21,27]. However, quantitatively reproducing these properties from vortex-only fields has proved elusive. In studies performed on pure Yang-Mills $SU(3)$ gauge fields, it is well known that vortices alone can only account for $\sim 62\%$ of the full string tension [19,23,29]. Similarly, the Landau gauge quark and gluon propagators calculated on vortex-only fields do not agree with their original values except after smoothing [24,27].

A natural next step for the vortex model is to examine how the presence of dynamical fermions impacts the structure of center vortices. Any subsequent shift in vortex structure can be measured by calculating observables arising from vortex-only and vortex-removed ensembles. In this paper, we perform the first such analysis and present a calculation of the static quark potential on vortex-modified ensembles in the presence of dynamical fermions. After identifying center vortices on the lattice, it is possible to isolate the contribution to the static quark potential from both the vortices alone and the original gauge field after vortex removal. This calculation reveals a significant shift in vortex structure induced by the presence of fermion loops in the vacuum fields and further reinforces the central role vortices play in producing the salient phenomena of QCD.

This paper is structured as follows. Section II outlines how center vortices are identified on the lattice. Section III introduces the calculation of the static quark potential through use of Wilson loops. Section IV describes the variational method used to calculate the static quark potential. Section V discusses the results of this work, introducing novel modifications to the standard Coulomb term. Section VI summarises our findings.

II. VORTEX IDENTIFICATION

In the continuum, center vortices are regions of an $SU(N)$ gauge field that carry flux associated with the center of the gauge group. These regions are "thick," meaning that in four dimensions they appear as three-dimensional volumes. On the lattice, we instead identify "thin" vortices that are correlated with the location of the physical thick vortices [9,30]. These thin vortices are two-dimensional sheets in four dimensions, which, when projected to three dimensions, appear as closed loops. Visualizations of these center vortices on the lattice have been presented in Ref. [31].

To identity center vortices on the lattice, we first transform each gauge field configuration to maximal center gauge

(MCG). This is done by finding the gauge transformation $\Omega(x)$ that serves to maximize the functional [23,29],

$$R = \frac{1}{VN_{\mathrm{dim}}n_c^2}\sum_{x,\mu}|\mathrm{Tr}U_\mu^\Omega(x)|^2. \tag{1}$$

This gauge transformation brings each link as close as possible to the center of the $SU(3)$ group. For $SU(3)$, the center of the group contains the three elements,

$$\mathbb{Z}_3 = \left\{\exp\left(\frac{m2\pi i}{3}\right)I, m = 0, \pm 1\right\}. \tag{2}$$

After fixing to maximal center gauge, the nearest center element is defined by finding the minimum difference in phase between $\mathrm{Tr}U_\mu(x)$ and one of the elements of $\mathbb{Z}_3$. $U_\mu(x)$ can then be projected onto this nearest center element to obtain the vortex-only configurations, $Z_\mu(x)$. The vortex-removed configurations are then defined as $R_\mu(x) = Z_\mu^\dagger(x)U_\mu(x)$.

For this work we make use of three ensembles of 200 $32^3 \times 64$ lattice gauge fields. Two of these are $(2+1)$ flavor dynamical ensembles from the PACS-CS Collaboration [32]. We choose the heaviest and lightest pion mass ensembles to provide the greatest differentiation as the physical point is approached. The pure gauge ensemble was generated with the Iwasaki action [33] at $\beta = 2.58$ with the intent of having a similar lattice spacing as the PACS-CS ensembles. This allows us to readily compare the full QCD results with those obtained from the pure gauge ensemble.

For each of these lattices, the MCG procedure above creates a corresponding set of vortex-modified fields. Throughout the rest of this work we refer to the three field types derived from a lattice ensemble as the

(i) Original, untouched (UT) fields, $U_\mu(x)$,
(ii) Vortex-only (VO) fields, $Z_\mu(x)$, and
(iii) Vortex-removed (VR) fields, $R_\mu(x)$.

The effectiveness of the MCG procedure can be seen in Fig. 1, which shows a histogram of center phases before and after MCG fixing on the pure gauge and lightest pion mass dynamical ensembles. Interestingly, we find that the pure gauge ensemble is more strongly peaked around the center phases, although the discrepancy is small, made visible by the logarithmic scale. A summary of the ensemble parameters can be found in Table I.

A. Parallel MCG fixing

Given the size of the lattices used in this work, it was necessary to implement a parallel version of the MCG algorithm, which proceeds as follows. To construct the maximal center gauge transformation $\Omega(x)$, it is sufficient to consider the nearest-neighbour contributions from $U_\mu(x)$

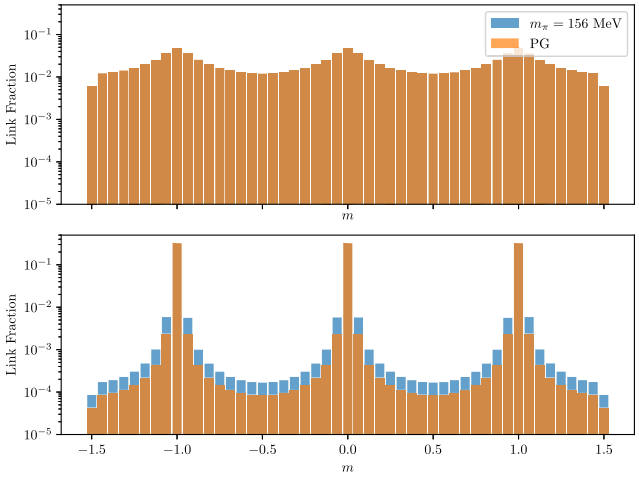

FIG. 1. A histogram showing the average phase distribution m of the pure gauge and lightest pion mass ensembles before (*top*) and after (*bottom*) maximal center gauge fixing. Note the logarithmic scale. In the top plot, the agreement is so close that the dynamical ensemble results are hidden by the pure gauge.

and $U_\mu(x-\hat{\mu})\,\forall\,\mu \in \{1,2,3,4\}$. For each x, one then seeks to maximise the local functional [34],

$$R(x) = \sum_\mu |\mathrm{Tr}\Omega(x)U_\mu(x)|^2 + \sum_\mu |\mathrm{Tr}U_\mu(x-\hat{\mu})\Omega(x)^\dagger|^2. \tag{3}$$

This is achieved by considering each of the three $SU(2)$ subgroups of $SU(3)$. $\Omega(x)_{\mathrm{SU}(2)}$ is then expressed as a linear combination of the $SU(2)$ generators $\vec{\sigma}$ such that

$$\Omega_{\mathrm{SU}(2)}(x) = g_4 I - i\vec{g}\cdot\vec{\sigma}. \tag{4}$$

This reduces Eq. (3) to a quadratic in $(g_4, \vec{g})$ subject to a unitarity constraint that can then be minimized via standard Lagrangian multiplier techniques. Once each of the three $SU(2)$ subgroups is iterated over once and $\Omega(x)$ has been constructed, it is then applied to the nearest-neighbor gauge links. The process is repeated for all other values of x and then iterated until a plateau in R [see Eq. (1)] is reached.

As $\Omega(x)$ depends only on its nearest-neighbors, we mask the algorithm to ensure that at any one time we consider only even or odd values of x, where even or odd is defined by whether $\sum_{\mu=1}^4 x_\mu$ is even or odd. We then distribute

TABLE I. A summary of the lattice ensembles used in this work [32].

Type	a(fm)	β	$\kappa_{\mathrm{u,d}}$	m_π(MeV)
Pure gauge	0.100	2.58	…	…
Dynamical	0.102	1.90	0.13700	701
Dynamical	0.093	1.90	0.13781	156

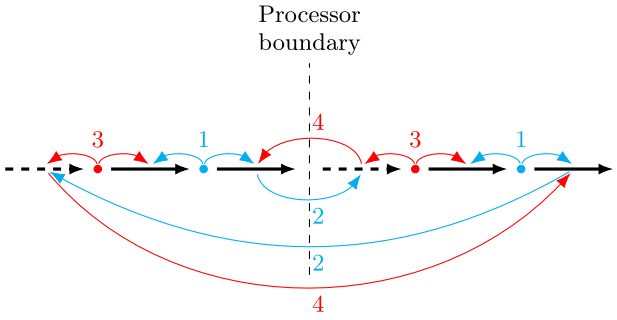

FIG. 2. MCG updating scheme for two processors. The update process is described in the text.

regular chunks of the lattice across processors with one shadowed plane in the directions along which the lattice has been subdivided. Once an even or odd sweep has been completed, the updated links are copied to adjacent processors so that they are available for the alternate sweep. A diagram illustrating this updating scheme for two processors distributed along one dimension is shown in Fig. 2.

The processor boundary is shown with the vertical dashed line. Gauge links are shown with solid black arrows and shadowed gauge links are shown with black dashed arrows. Shown is the update process starting with the even sites (blue circles) followed by the odd sites (red circles):

(1) The gauge links adjacent to the even sites are updated with the gauge transformation $\Omega(x)$.
(2) The updated links along the boundary are copied to the relevant shadowed locations.
(3) The gauge links adjacent to the odd sites are updated.
(4) The updated shadowed links are copied to the relevant locations.

This method of parallel implementation requires a slightly greater number of overall sweeps than the serial implementation, as each update does not have the fully propagated information that would be carried by a serial process starting from one corner of the lattice. However, it has a number of advantages. Most apparent is the real-time reduction in wall time, as the parallel implementation scales very well thanks to minimal cross-processor memory requirements. Additionally, there is no directionality in this implementation as each site only sees its neighbors during each sweep. This suppresses any inconsistency arising from choice of start point or order of iteration. Given that each site is only affected by its nearest neighbors, this implementation also has the desirable property of being agnostic to the number of processors used in the calculation.

III. STATIC QUARK POTENTIAL

The static quark potential provides a measurement of the potential between two massive, static quarks at a separation

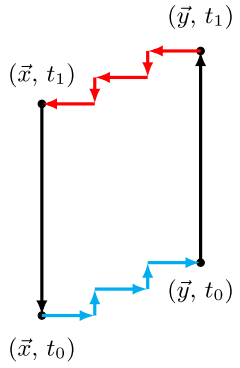

FIG. 3. Diagram of a Wilson loop. Shown are the forward (blue) and backward (red) spatial paths where different levels of smearing are used to create our variational matrix. Links in the positive temporal direction are oriented vertically upwards.

distance r. On the lattice, the static quark potential can be obtained by considering the Wilson loop,

$$W(r,t) = \mathrm{Tr} R(\vec{x},t_0)T(\vec{y},t_0)R^\dagger(\vec{x},t_1)T^\dagger(\vec{x},t_0), \quad (5)$$

that has two spatial paths connecting points $\vec{x}$ and $\vec{y}$ satisfying $|\vec{y}-\vec{x}| = r$ via the shortest set of links on the lattice. The forward spatial path $R(\vec{x},t_0)$ is separated from the backward spatial path $R^\dagger(\vec{x},t_1)$ by the temporal extent of the loop, $t_1 - t_0 = t$. The loop is closed via the static quark propagators $T(\vec{y},t_0)$ and $T^\dagger(\vec{x},t_0)$, which correspond to the product of links in the positive and negative temporal directions, respectively. A diagram of this Wilson loop construction is shown in Fig. 3.

When the spatial separation extends off axis to encompass displacements in more than one spatial direction, a diagonal path is chosen to reduce rotational lattice artifacts. An integer step size vector $\vec{s}$ is initialized by taking the spatial separation $\vec{r}$ and dividing out the smallest element. If the two largest elements of $\vec{s}$ are both greater than 1, then these are divided by the smaller of the two so that the step size vector $\vec{s}$ has at most one element that is greater than 1. The spatial link path is constructed by cycling between the spatial directions $\hat{\jmath}$ with step size s_j. When the total displacement r_j in a direction $\hat{\jmath}$ has been reached we set the step size $s_j = 0$. This is perhaps most easily understood with an example. For $\vec{r} = (6,3,2)$, then the initial step size vector $\vec{s} = (3,1,1)$. The path $\vec{r}$ is traversed by starting at $\vec{x}$ and cycling through the steps $\vec{s} = (3,1,1)$ twice, then updating $\vec{s} = (0,1,0)$ to the remaining displacement to reach the end point $\vec{y}$.

The expectation value of the Wilson loop is connected to the static quark potential V^α for state α via the expression,

$$\langle W(r,t)\rangle = \sum_\alpha \lambda^\alpha(r)\exp\left(-V^\alpha(r)t\right). \quad (6)$$

Here, α enumerates the sum over energy eigenstates. This expectation value in Eq. (6) is taken not only over the lattice ensemble, but over the range of spatial paths that provide the same r value. In this work, we consider a maximum of 16 on axis points, and a range of 0 to 3 off axis points. The temporal extent considered has a maximum of $t = 12$ for the untouched and vortex-removed ensembles, and a maximum of $t = 32$ for the vortex-only. The larger value for the vortex-only ensemble is used because the onset of noise occurs much later, and we find better plateau fits using this extended range.

Due to the cubic symmetry of the lattice, when considering a link path between two spatial points separated by a given displacement vector $\vec{r} = \vec{y} - \vec{x}$ it is possible to permute the three spatial coordinates and obtain the same value for the separation $r = |\vec{r}|$. Averaging over these permutations allows for further improvement of statistics for the corresponding Wilson loop and better extraction of the ground state.

IV. VARIATIONAL ANALYSIS

The analysis of the static quark potential is susceptible to excited state contamination and signal to noise challenges. In particular, the dynamical ensembles are typically noisier at a given lattice spacing compared to the pure gauge case. To better extract the ground state potential at earlier Euclidean time, we create a correlation matrix by introducing different levels of smearing along the two spatial edges of the Wilson loops describing the profile of the flux tube,

$$W_{ij}(r,t) = \mathrm{Tr} R_i(\vec{x},t_0) T(\vec{y},t_0) R_j^\dagger(\vec{x},t_1) T^\dagger(\vec{x},t_0). \quad (7)$$

Here the forward and backwards paths $R_i(\vec{x},t_0)$ and $R_j^\dagger(\vec{x},t_1)$ are constructed using links that have respectively had i and j sweeps of spatial APE smearing [35] applied, with a smearing parameter of $\alpha = 0.7$. For the untouched and vortex-removed ensembles, the $SU(3)$ projection component of the APE smearing algorithm is performed using the unit-circle projection method described in Ref. [36].

The vortex-only ensembles present some difficulties in the application of standard smearing algorithms, as highlighted by recent work [37] that delved into the difficult question of smoothing $SU(3)$ center vortex configurations. We employ these findings to best extract the static quark potential, starting with a brief summary of the relevant results from this study.

It was shown in Ref. [37] that gauge-equivariant smoothing (such as unit-circle projection) when applied to $SU(3)$ vortex-only configurations results in either no effect or a swapping of the center phase to another element of $\mathbb{Z}_3$, spoiling the center vortex structure. The use of a nonanalytic reuniterization performed via a MaxRe Tr method [38] can circumvent this issue; however it is subject to strict constraints on the smearing parameter α.

The primary cause of the difficulties in smoothing vortex fields arises from the proportionality of the vortex links to the identity. To alleviate this issue, we apply the novel centrifuge preconditioning method that was introduced in Ref. [37], but only to the spatial links used to construct the Wilson loop. Centrifuge preconditioning introduces a small perturbation that rotates the vortex links away from the center group $\mathbb{Z}_3$ whilst maintaining the vortex structure. This is then followed by application of APE smearing at smearing fraction $\alpha_{\mathrm{APE}} = 0.7$ using MaxRe Tr reuniterization to generate the variational basis for vortex-only configurations.

For N choices of smearing sweeps, we obtain the $N \times N$ correlation matrix,

$$\begin{aligned} G_{ij}(r,t) &= \langle W_{ij}(r,t) \rangle \\ &= \sum_\alpha \lambda_i^\alpha \lambda_j^{*\alpha} \exp\left(-V^\alpha(r) t\right), \end{aligned} \quad (8)$$

where the i, j indices enumerate the N smearing variations on the initial and final spatial edges of the Wilson loop respectively. The complex scalars λ_i^α and $\lambda_j^{*\alpha}$ represent the coupling of each smeared leg of the Wilson loop to the static quark potential V^α. Note that in the following we choose to suppress the implied r dependence of G_{ij} and V for clarity.

Presuming that the signal is dominated by the N lowest energy states, such that $\alpha \in [0, N-1]$, we wish to find a basis $\mathbf{u}^\alpha$ such that,

$$G_{ij}(t) u_j^\alpha = \lambda_i^\alpha z^{*\alpha} e^{-V^\alpha t}, \quad (9)$$

where $z^{*\alpha} = \sum_i \lambda_i^{*\alpha} u_i^\alpha$ is now the coupling between this new basis and the energy eigenstate $|\alpha\rangle$. Note that for the remainder of this paper we adopt the convention that repeated Latin indices are to be summed over whilst repeated Greek indices are not. Equation (9) is equivalent to requiring that

$$\lambda_i^{*\alpha} u_i^\beta = z^{*\alpha} \delta^{\alpha\beta}. \quad (10)$$

Noting that the time dependence in Eq. (9) depends only on the exponential term, we can consider stepping forward in time by some amount Δt such that,

$$\begin{aligned} G_{ij}(t_0 + \Delta t) u_j^\alpha &= \lambda_i^\alpha z^{*\alpha} e^{-V^\alpha (t_0 + \Delta t)} \\ &= e^{-V^\alpha \Delta t} G_{ij}(t_0) u_j^\alpha. \end{aligned} \quad (11)$$

This recursive relationship is precisely a generalized eigenvalue problem, which can be solved via standard numerical techniques to obtain the eigenvectors $\mathbf{u}^\alpha$.

An identical argument can be made for the left eigenvectors $\mathbf{v}^\alpha$, such that they satisfy

$$v_i^\alpha G_{ij}(t) = z^\alpha \lambda_j^{*\alpha} e^{-V^\alpha t}, \tag{12}$$

and hence,

$$v_i^\alpha G_{ij}(t_0 + \Delta t) = e^{-V^\alpha \Delta t} v_i^\alpha G_{ij}(t_0). \tag{13}$$

Making use of Eqs. (9) and (13), we find that

$$v_i^\alpha G_{ij}(t) u_j^\beta = z^\alpha z^{*\beta} \delta^{\alpha\beta} e^{-V^\alpha t}. \tag{14}$$

As such, we define the eigenstate-projected correlator,

$$\begin{aligned} G^\alpha(t) &= v_i^\alpha G_{ij}(t) u_j^\alpha \\ &= z^\alpha z^{*\alpha} e^{-V^\alpha t}, \end{aligned} \tag{15}$$

and extract the potential by computing the log-ratio,

$$V_{\text{eff}}^\alpha(t) = \ln\left(\frac{G^\alpha(t)}{G^\alpha(t+1)}\right), \tag{16}$$

to obtain the static quark potential. We then consider constant fits to the lowest energy state, $V_{\text{eff}}^0(r,t)$.

We use a 4×4 correlation matrix for the untouched and vortex-removed ensembles, with a basis constructed from 6, 10, 18 and 30 sweeps of APE smearing. For the vortex-only ensembles, even with centrifuge preconditioning and MaxReTr reuniterisation applied, the configurations are still slow to vary as a function of smearing sweeps. As a consequence of this, we choose a 2×2 correlation matrix with 2 and 60 sweeps of APE smearing to provide a meaningful distinction between the basis elements.

In regards to the choice of variational parameters for the original and vortex-removed ensembles, we find that increasing Δt minimally affects the level of noise, whilst providing slight improvement in ground state identification. Thus, we choose a larger value of $\Delta t = 3$. Selecting larger values of t_0 introduces substantial noise into the results obtained from these ensembles, so we maintain $t_0 = 1$ on these ensembles.

Selection of variational parameters is slightly different on the vortex-only ensembles. For the diagonal correlators, $G_{ii}(t)$, where source and sink match and all states should contribute positively, i.e., $\lambda_i^\alpha \lambda_i^{*\alpha} > 0$, the effective mass approaches from below. This is indicative of short-distance positivity violation arising in the process of center projection. In the context of a variational analysis, we extend t_0 to the greatest feasible degree to avoid the region of positivity violation at early times [39]. Indeed, our focus is on understanding whether projected center vortices can capture the long-distance, nonperturbative features of QCD. To this end, we choose $(t_0, \Delta t)$ to be (5,4), (4,5) and (4,2) for the pure gauge, $m_\pi = 701$ MeV, and $m_\pi = 156$ MeV vortex-only ensembles respectively. The difference in variational parameters between the ensembles arises from when the onset of noise dominates the signal.

To calculate uncertainties, we perform a third-order single-elimination jackknife calculation [40]. Fit window selection is performed to prioritise finding the earliest appropriate value of t_{min}, in a method similar to that outlined in Ref. [41]. As such, we select an initial t_{max} to be the largest value maintaining $V(r, t_{\text{max}}) > \Delta V(r, t_{\text{max}})$, where $\Delta V(r, t_{\text{max}})$ is the jackknife uncertainty in $V(r, t_{\text{max}})$. An initial value of $t_{\text{min}} = t_0 + 2$ is chosen. t_{max} is then decreased until a covariance fit over the range $[t_{\text{min}}, t_{\text{max}}]$ produces a χ^2 per degree of freedom, $\tilde{\chi}^2$, of less than 1.3. If no such t_{max} is found, t_{min} is increased by one lattice unit, and the procedure is repeated. The on axis results of this fitting procedure are shown for the lightest pion mass

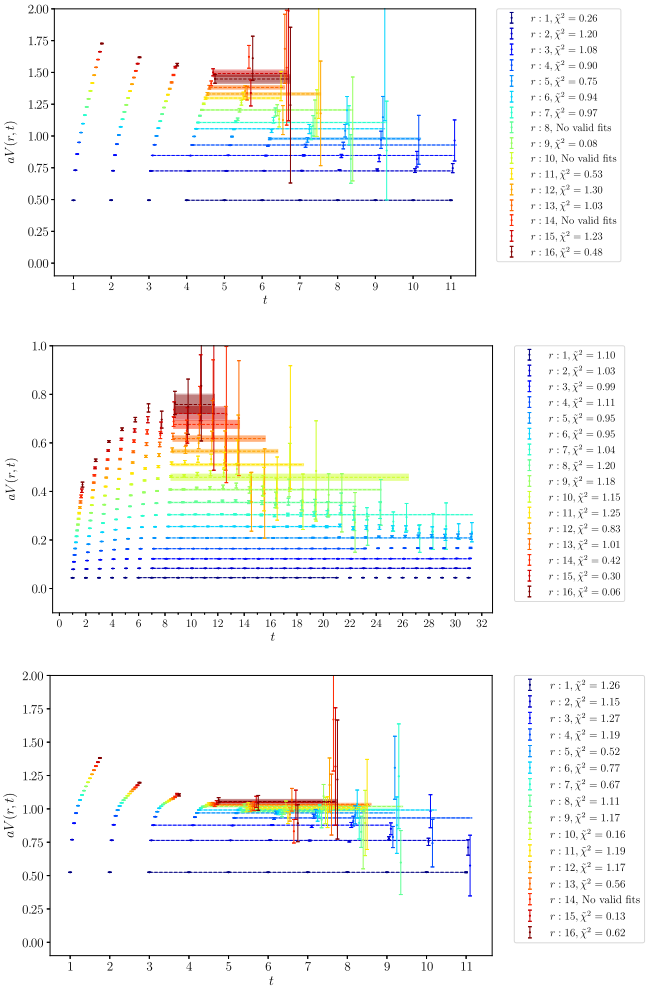

FIG. 4. The on axis projected effective mass from the original $m_\pi = 156$ MeV ensemble. Results are shown for the original (*top*), vortex-only (*middle*) and vortex-removed (*bottom*) ensembles. The selected fit window that meets the $\tilde{\chi}^2$ criteria as described in the text is shown as the dashed lines. The shaded region shows the jackknife error on the fit. Points at the same value of t are horizontally offset for visual clarity. Any points with a relative error greater than 50% are excluded from the plot.

TABLE II. The ansätze used for the three ensembles.

Type	Ansatz	Functional form
Untouched	Cornell	$V(r) = V_0 - \alpha/r + \sigma r$
Vortex-only	Linear	$V(r) = V_0 + \sigma r$
Vortex-removed	Coulomb	$V(r) = V_0 - \alpha/r$

ensemble in Fig 4. Once fits have been performed for all values of r, we select a single fit window with a width of at least two lattice units (i.e., at least three time values) such that it is typically encompassed by the range of fit windows found for each value of r.

After the potential $V(r)$ is determined, we then perform functional fits to the UT, VO and VR potentials. The Ansätze used for each ensemble are given in Table II. The functional fits take into account the full covariance matrix, and error regions are constructed via repetition of the fits on the jackknife ensembles. The selection of the range $[r_{\text{min}}, r_{\text{max}}]$ to fit over is performed in a manner similar to the fit window selection for the effective mass. For the UT and VR ensembles we initialize r_{min} to the lowest available value, as we find that our window selection method naturally avoids the short-range region that is plagued by lattice systematics. To explicitly avoid this region for the vortex-only potential, we initialize $r_{\text{min}} = 5$ for these ensembles. r_{max} is initialized to the largest available value on all ensembles. Over this initial range, the functional fit is performed and the χ^2 per degree of freedom, $\tilde{\chi}^2$, is calculated. If it is greater than 1.3 then r_{max} is reduced by $\Delta r = 0.2$, and the fit is repeated. If $r_{\text{max}} - r_{\text{min}} < 3$, r_{max} is reset to its maximum extent and r_{min} is increased by $\Delta r = 0.2$. In our plots, points that are included in the fit are shown in solid colors, whereas points excluded from the fit are shown as faded.

We also present plots of the local slope calculated from a series of linear fits taken over a sliding r window of width 4 lattice units. Each fit window is successively shifted in increments of $\Delta r = 0.4$ lattice units, with the fitted slope plotted at the leftmost edge. We find that $r = 5$ is approximately where the onset of linearity begins, and hence we begin our sliding windows from this value. The excluded short-distance region is greyed out in the plots presented. This procedure for obtaining the local slope provides a simple method for gauging the linearity of the potential over a range of distances.

V. RESULTS

We now present the results for the static quark potential. To verify that our variational technique is appropriate, we first calculate the vortex-only potential from the $m_\pi = 156$ MeV ensemble without a variational method to check if the results from the variational analysis are consistent and represent an improvement. Given the similarity of the lattice spacing on our three ensembles, summarized in Table I, we will consider r in lattice units for the remainder of this work. We find that the fitted string tension is lower after a variational analysis, with $\sigma_{\text{VO}} = 0.0484(4)$ and $\sigma_{\text{VO}} = 0.0490(4)$ with and without variational analysis respectively. Additionally, the effective mass plateau fits occur at earlier times with the variational analysis, especially at larger r values. This suggests that the variational analysis is appropriate and represents an improvement over the naive method.

We show the VO potential with and without variational analysis in Fig. 5. Fitting is performed via the method outlined in the previous section. We observe from the local slope plot that the long range potential is similar across both methods. The fact that the differences are so slight is a testament to the excellent signal-to-noise ratio in vortex only ensembles and the subsequent access to large Euclidean times in the Wilson loops. Nevertheless, the use of a variational method does improve the onset of lower-lying plateaus and is thus preferred.

As we are studying gauge fields that include dynamical fermions, this gives rise to the possibility of string breaking. However, it is well known that there is poor overlap between the infinitely heavy static quark state and the heavy-light meson-meson state which arises from the string breaking transition [42]. To identify string breaking, it is instead necessary to include operators for heavy-light meson-meson states in the correlation matrix, as done in Refs. [42,43].

The purpose of the variational analysis employed here is to ensure accurate identification of the ground state potential to enable comparison between the original and

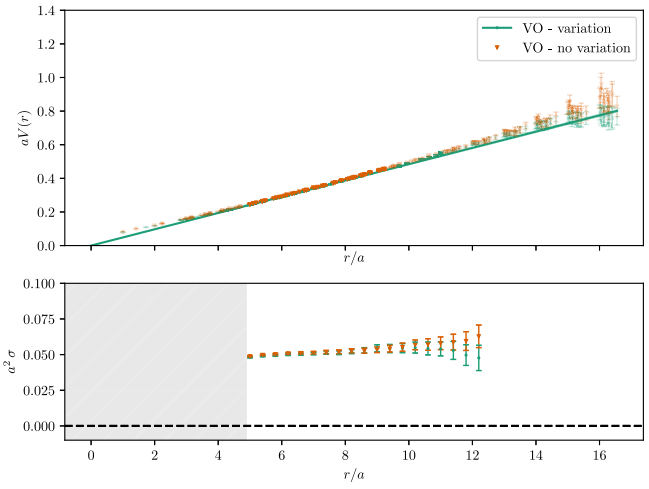

FIG. 5. A comparison of the vortex-only potential from the $m_\pi = 156$ MeV ensemble extracted after no spatial smearing and our variational method as described in the previous section. V_0 is set to 0 for both sets of results. The functional fit for the variational results is also plotted. We observe a similar potential for both choices; however the linearity of the fit is improved after a variational method, with a larger range of points meeting the fit criteria discussed in the text.

vortex-modified ensembles. Our basis does not include any of the appropriate operators to directly observe string breaking in this analysis. The inclusion of these operators requires inversion of the fermion matrix, which poses technical difficulties on the vortex-only fields due to their rough nature. These difficulties can be ameliorated with the use of sophisticated smoothing techniques such as those described in Ref. [37]. However, this would introduce a level of complication to the variational analysis beyond what is necessary for this study and is left to future work.

A. Standard potential fits

The static quark potential from the pure gauge ensemble is presented in Fig. 6. Our results coincide with findings from previous studies [19,23,29]. The untouched potential is Coulomb-like at short distances whilst becoming linear as r increases. We observe that the vortex-removed and vortex-only potentials of Table II qualitatively capture these regimes respectively. Vortex removal results in Coulomb-like behavior at short distances, with approximately constant behavior at moderate to large r indicating the absence of a linear string tension. We do note, however, that the Coulomb term provides a poor representation of the VR results at large r. Contrasting the vortex-removed results, we observe that the vortex-only ensemble features no $1/r$ behavior, instead displaying a linear potential with a slope of approximately 62% that of the original ensemble.

The fitted string tension values from the untouched and vortex-only ensembles are presented in Table III. The ratio of the vortex-only string tension to the untouched string tension is shown in the third column. We see that while the vortex field from the pure gauge background is only able to recreate 62% of the untouched string tension, in the presence of dynamical fermions there is a different story. The fitted vortex-only string tension increases upon the introduction of dynamical fermions at the heaviest pion mass. At $m_\pi = 701$ MeV the fitted string tension for the vortex-only and untouched fields are nearly equal, whereas on the lightest ensemble at $m_\pi = 156$ MeV the fitted string tension on the vortex-only field exceeds the untouched value by about 25%.

TABLE III. The fitted string tensions from the vortex-only and untouched ensembles, and their respective ratios.

m_π(MeV)	$a^2\sigma_{\mathrm{VO}}$	$a^2\sigma_{\mathrm{UT}}$	$\sigma_{\mathrm{VO}}/\sigma_{\mathrm{UT}}$
Pure gauge	0.0344(9)	0.0558(3)	0.62(2)
701	0.0570(7)	0.0537(7)	1.06(2)
156	0.0484(4)	0.0386(1)	1.25(3)

What is clear is that the presence of dynamical fermions significantly alters the texture of the vortex vacuum, even at an unphysically large quark mass. The question then posed is how best to shed some light on the nature of this "sea change." Figure 7 shows the static quark potential results for the heavy dynamical ensembles, with $m_\pi = 701$ MeV. Examining the local slope as it varies with r provides some insight. Note that the lattice spacings (as set by the Sömmer scale) of the three ensembles listed in Table I are approximately the same, so it is reasonable to make broad comparisons in the slopes of the potentials.

As before, vortex removal captures the short-range physics while absenting any linear rise associated with a confining potential. Strikingly, the vortex-only field projected from the dynamical ensemble now fully reproduces the long-range potential. This is best observed in the

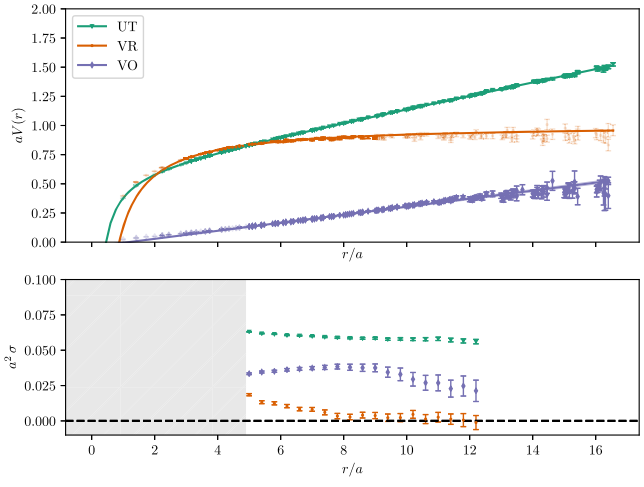

FIG. 6. The static quark potential as calculated from the pure Yang-Mills ensemble. Points are obtained from the variational analysis and solid lines show the fitted Ansatz for each ensemble. The choice of Ansatz is as described in Table II. Faded points indicate that this point was not included in fitting the Ansatz, as described in the text. The lower plot shows the fitted local slope of a forward-looking sliding linear window from r to $r + 4a$.

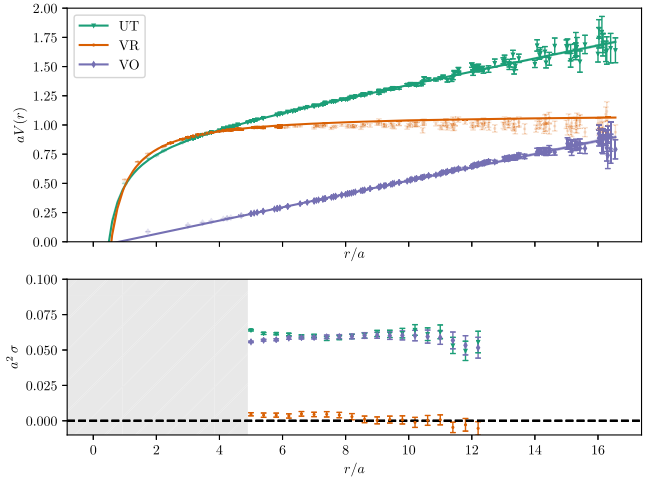

FIG. 7. The static quark potential as calculated from the $m_\pi = 701$ MeV ensemble, with features as described in Fig. 6.

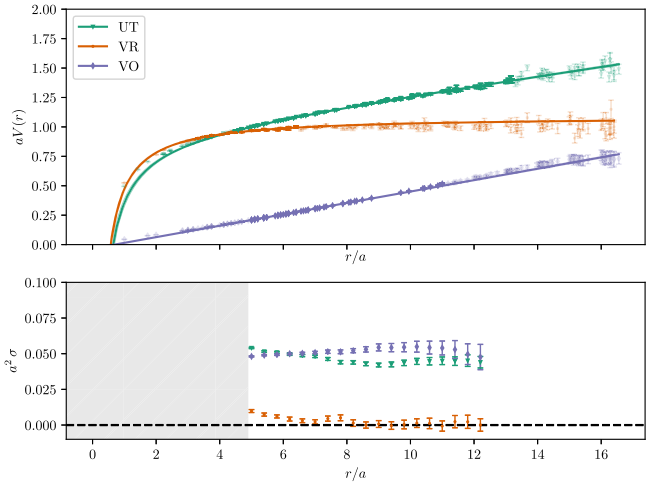

FIG. 8. The static quark potential as calculated from the $m_\pi = 156$ MeV ensemble, with features as described in Fig. 6.

moving local slope displayed in the lower panel of Fig. 7. The more precise fitted string tension σ shows approximate agreement as reported in Table III. This will be discussed in greater detail in the next subsection.

Finally, we present the static quark potential on the ensemble with the lightest pion mass of 156 MeV in Fig. 8. Here we observe the untouched and vortex-only slopes crossover, with approximate agreement of the local slope in the region $r \in [5.5, 7]$. As we extend to larger distances, we observe that the vortex-only string tension exceeds the original value. This overestimation is corroborated by the fit values, where the value of σ reported in Table III is approximately 25% larger than the untouched.

The unanticipated overestimation of the VO string tension at the lightest mass gives an indication that there is some additional physics that is not being accounted for. A hint as to the possible answer is revealed in the vortex-removed fits. Specifically, the standard Coulomb term retains a residual increase in strength at moderate to large r that does not match the approximately constant behavior of the vortex-removed results. The slow rise present in the standard Coloumb term could also interfere with the fitted linear term coefficient, resulting in an underestimation of the string tension in the UT results where both the Coulomb and string-tension terms are present.

Table IV shows that as pion mass decreases, the fitted value of the Coulomb term coefficient, α, on the UT ensembles increases. This would then enhance possible contamination of the fitted UT string tension resulting from physics absent from the standard Coulomb term, amplifying the discrepancy between the original and vortex-only string tensions. This motivates modifications to the Coulomb term that we introduce in the next section in order to obtain better descriptions of the lattice results and more accurate estimates of the string tension.

B. Modified Coulomb potential fits

We have seen the difficulty in fitting the Coulomb term parameter, α, in our Ansatz to a wide range of values on the dynamical ensembles. At the shortest distances, there is a well-known difficulty associated with fitting α for both the original and vortex-removed ensembles [44], stemming from the small statistical errors present at short range coupled with the presence of finite lattice-spacing systematics.

It is possible to apply a lattice correction to the Coulomb term to compensate for these short-distance artifacts [45,46]. However, here we are mainly concerned with the long distance behavior and adopt the simple solution of excluding small values of the static quark separation r from our fits.

A more serious limitation in the fit functions used above is revealed upon vortex removal. The standard Coulomb term is only able to describe the vortex-removed results over a limited range. This demonstrates a need for a modified fit function in order to describe the large r behavior of the vortex-removed potential.

TABLE IV. Results of the standard static quark potential fits to the three ensembles. The fit parameters are described in Table II, and $\tilde{\chi}^2$ denotes the χ^2 per degree of freedom.

Type	$(r_{\min}, r_{\max})$	$\tilde{\chi}^2$	aV_0	α	$a^2\sigma$
			Pure gauge		
UT	(3.10, 16.55)	1.12	0.608(3)	0.286(7)	0.0558(3)
VR	(3.00, 9.05)	1.23	1.010(2)	0.881(7)	…
VO	(5.00, 16.40)	0.97	−0.041(4)	…	0.0344(9)
			$m_\pi = 701$ MeV		
UT	(3.10, 16.55)	1.30	0.847(7)	0.42(1)	0.0537(7)
VR	(3.00, 6.55)	1.30	1.092(4)	0.59(1)	…
VO	(5.00, 16.55)	1.03	−0.047(4)	…	0.0570(7)
			$m_\pi = 156$ MeV		
UT	(4.40, 13.25)	1.29	0.93(1)	0.61(4)	0.0386(1)
VR	(3.10, 5.40)	1.28	1.106(5)	0.68(2)	…
VO	(5.00, 11.15)	1.28	−0.033(2)	…	0.0484(4)

The decoupling of the static quark potential into the vortex-removed and vortex-only components also provides us with an opportunity. Specifically, the large r behavior of the untouched potential is dominated by the linear string tension. The dominance of the linear term at large r hides any subleading effects.

The vortex-only component of the potential is well described by a linear string tension. The origin of the confining string tension is attributed to nontrivial vacuum structure, with the center-vortex model of course being the most pertinent to this study. On the other hand, the vortex-removed potential does not possess a string tension as testified by the absence of a linear slope. This provides us with a chance to model effects that would otherwise be obscured by the rising linear string tension.

The first modified Ansatz we propose is novel, with a model based on antiscreening of the Coulomb potential,

$$V_{\mathrm{as}}(r) = V_0 - \frac{\alpha}{1 - e^{-\rho r}}. \tag{17}$$

The Laurent series of this function is dominated by the lowest order term $\tilde{\alpha}/r$ at short distances providing a Coloumb-like potential, where the effective Coulomb coefficient is $\tilde{\alpha} = \alpha/\rho$. Antiscreening implies that the strong coupling constant $\alpha_s(r)$ increases with increasing separation between two test colour charges. If α_s increases as r increases, this will have the effect of counteracting decreasing behavior of the $1/r$ term.

The specific form of the Ansatz we have chosen here is motivated by the observation of the flat, constantlike behavior of the vortex-removed potential at large distances. Specifically, at large r the exponential in the denominator of Eq. (17) tends to zero, such that a constant value $V_{\mathrm{as}} \to V_0 - \alpha$ is rapidly approached as r increases. The implication of this is that the running coupling of α_s is approximately linear in r within the fitted region. Previous lattice studies of the running of the strong coupling do show an increase in α_s with the separation r, although they are limited in the applicable range of scale (up to ~0.5 fm) [45,47,48]. Importantly, the form of Eq. (17) is controlled such that the large r behavior cannot describe a rising linear potential tension and hence should not interfere with a fitted string tension.

Intuitively, antiscreening can be understood by noting that at short distances gluons carry color charge away from a quark or antiquark such that the effective color charge within a given radius is diluted, leading to asymptotic freedom at short distances [49]. We know from previous studies of the pure-gauge vortex-removed gluon propagator that flat behavior consistent with asymptotic freedom is observed at large q^2 [27]. We also know that antiscreening arises from the non-Abelian nature of the gluon field, and as the vortex-removed field remains non-Abelian it seems reasonable to postulate that antiscreening will still be present in the absence of confinement.

Of course there are more sophisticated calculations of the running of α_s [48,50–55], but these have limited applicability here, either due to the limited range of perturbation theory in QCD or being inspired by the string tension. It is not clear how these apply to vortex-modified fields. Here we choose instead to simply model the observed behavior of the vortex-removed potential.

We also consider an alternative model to fit the vortex-removed results. The second modified Ansatz we propose is a screened Coulomb potential, commonly known as the Yukawa potential,

$$V_{\mathrm{sc}}(r) = V_0 - \frac{\alpha}{r} e^{-\rho r}. \tag{18}$$

Once again this has a Coulomb-like $1/r$ behavior at small r. At large r the exponential term has the effect of turning off the Coulomb interaction such that $V_{\mathrm{sc}} \to V_0$ as r increases.

One interpretation of the Yukawa model in this context is that the gluon dynamically acquires an effective mass ρ in the infrared. As a nonzero gluon mass is forbidden at the Lagrangian level by gauge invariance, this mechanism must be dynamical and scale-dependent. Indeed, the dynamical generation of an effective gluon mass has been proposed elsewhere as a possible mechanism for the gluon propagator to take a finite value in the infrared limit [56–60].

It must be emphasized that the finiteness of the gluon propagator in the infrared limit is distinct to the presence (or absence) of confinement. The signature of confinement is dependent on the nature of the running of the gluon mass. Specifically, confinement is associated with an inflection point or turnover in the gluon propagator, which in turn implies the running gluon mass should not be constant. We know that vortex-removed theory does not generate a string tension and hence is nonconfining. Introducing the possibility of a constant effective gluon mass at a finite scale would model the vortex-removed potential in a way which is separate to any confinement mechanism.

We now turn to the results from our modified Coulomb Ansätze. Table V presents the fit parameters, with the resulting potentials illustrated in Fig. 9. We see that both V_{as} and V_{sc} are able to describe the vortex-removed results well, with similar values for the reduced χ^2. At first glance it seems somewhat counterintuitive that both an antiscreened and screened model are able to describe the same results. Numerically, this is possible because of the interplay between the V_0 and α. Both Ansätze approach a constant value in the large r limit, with $V_{\mathrm{as}} \to V_0 - \alpha$ and $V_{\mathrm{sc}} \to V_0$ respectively.

We see that both modified Ansätze provide a superior fit to the vortex-removed results when compared to the standard Coulomb Ansatz, allowing the fit window to extend to the maximum available r_{max}. In all cases the fitted value of r_{min} is less than or equal to the standard potential fits, indicating that the modifications made to the Coulomb

TABLE V. Results of the functional fits to the modified Ansätze described in the text. The values of ρ for the untouched ensembles are fixed to the value obtained from the corresponding vortex-removed fit.

Type	$(r_{\min}, r_{\max})$	Fit function	$\tilde{\chi}^2$	aV_0	α	$a^2\sigma$	ρ
		Pure gauge					
VR	(2.90, 16.55)	V_{as}	1.10	1.20(3)	0.27(3)	…	0.28(2)
VR	(2.90, 16.55)	V_{sc}	1.13	0.931(5)	1.01(3)	…	0.15(2)
UT	(3.00, 16.55)	$V_{\text{as}} + \sigma r$	1.16	0.652(4)	0.081(2)	0.0572(3)	0.28
UT	(3.00, 16.55)	$V_{\text{sc}} + \sigma r$	1.19	0.573(2)	0.301(7)	0.0572(3)	0.15
		$m_\pi = 701$ MeV					
VR	(1.80, 16.55)	V_{as}	0.97	1.42(2)	0.42(3)	…	0.53(2)
VR	(1.80, 16.55)	V_{sc}	1.01	1.005(2)	0.85(2)	…	0.31(2)
UT	(3.00, 16.55)	$V_{\text{as}} + \sigma r$	1.29	1.02(1)	0.259(9)	0.0588(5)	0.53
UT	(3.00, 16.55)	$V_{\text{sc}} + \sigma r$	1.30	0.761(4)	0.54(2)	0.0585(5)	0.31
		$m_\pi = 156$ MeV					
VR	(3.00, 16.40)	V_{as}	1.18	1.48(6)	0.48(6)	…	0.51(4)
VR	(3.00, 16.40)	V_{sc}	1.18	1.009(3)	1.05(8)	…	0.33(3)
UT	(4.40, 9.25)	$V_{\text{as}} + \sigma r$	1.28	1.17(4)	0.37(3)	0.0459(9)	0.51
UT	(4.40, 9.25)	$V_{\text{sc}} + \sigma r$	1.28	0.804(7)	0.84(7)	0.0457(9)	0.33

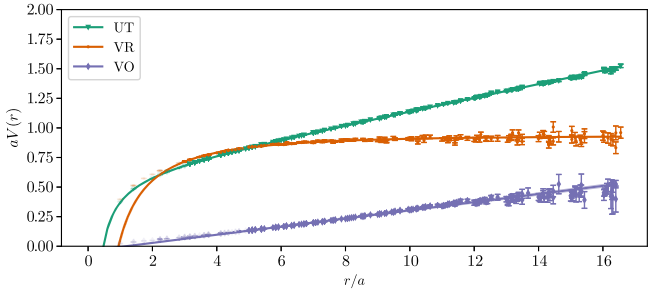

(a) Pure gauge, V_{as} fit.

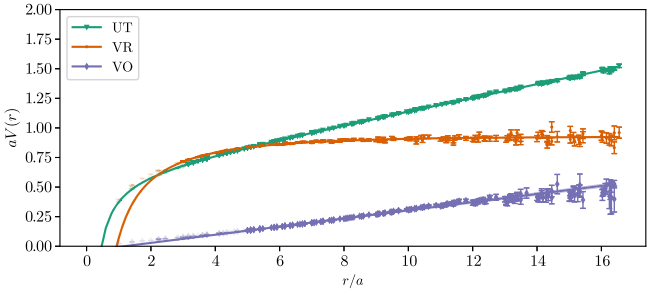

(b) Pure gauge, V_{sc} fit.

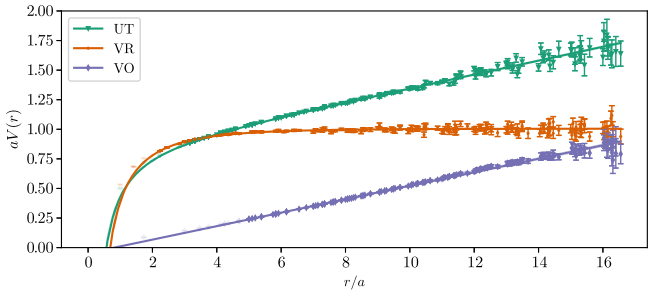

(c) $m_\pi = 701$ MeV, V_{as} fit.

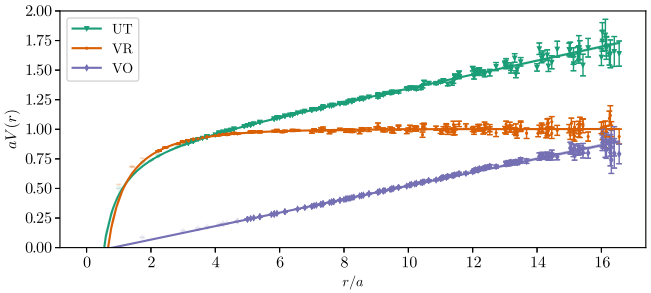

(d) $m_\pi = 701$ MeV, V_{sc} fit.

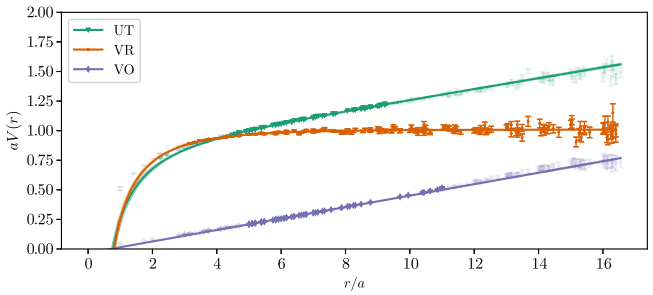

(e) $m_\pi = 156$ MeV, V_{as} fit.

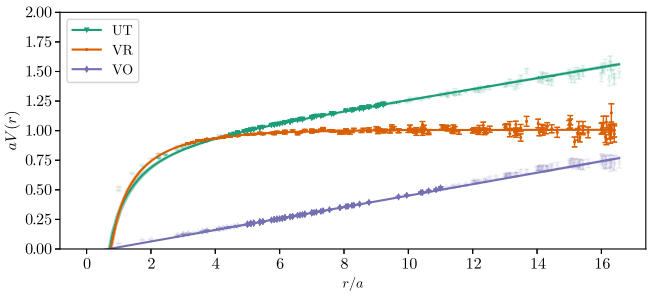

(f) $m_\pi = 156$ MeV, V_{sc} fit.

FIG. 9. Fits to the lattice results for the potentials using the modified Coulomb term functions V_{sc} and V_{as} described in the text. The vortex-removed results are now described well by the modified potentials.

terms are still able to account for the short distance behavior of the potential up to the presence of lattice artifacts.

Having verified that our modified Ansätze are successfully able to describe the vortex-removed potential results at large r, we can then use this information to improve our fits to the untouched results. This is accomplished by fixing ρ to be the value obtained from the corresponding vortex-removed ensemble, then adding a linear term to accommodate the string tension component of the untouched potential. The motivation behind fixing ρ is that the cleanest fit value for this parameter will be obtained in the absence of a string tension term which will dominate the large r behavior. Indeed, we find that if left as a free parameter ρ is poorly constrained by the untouched potential fits due to the presence of the dominating linear term.

The fits to the untouched ensembles are of comparable range and $\tilde{\chi}^2$ to the original Cornell fits; however when we look at the ratio of the vortex-only string tension to the untouched, shown in Table VI, we see the significant impact the modified Coulomb terms play. The untouched string tension on the pure gauge ensemble is similar to the Cornell fit value, however on the dynamical ensembles the string tension is increased due to cleanly removing the contamination from the slow rise in the standard Coulomb term at moderate to large r. Remarkably, this results in agreement between the vortex-only and untouched string tensions on both dynamical lattices, as seen by the corresponding ratios taking values close to unity in Table VI.

The fits to the results are unable to distinguish between the two modified ansätze. Indeed, the resulting improvements to the untouched potential fits result in values for the string tension that are essentially identical. We also tested an n-tuple form factor, $(1+(r/\rho)^n)^{-1}$, to suppress the Coulomb term at large r, and this provided a similar result. This gives us confidence that any systematic errors arising from the modified Coulomb terms are minimal in the final string tensions reported.

The physical arguments provided for the two modified Ansätze are simply to demonstrate some plausible mechanisms that might underpin their empirically motivated forms. Due to the interplay between α and V_0 it is likely that more than one effect will contribute to the fitted values. With a high-precision scaling analysis, a future examination may be able to resolve the physics represented by these modifications. The key result here is that by successfully modeling the observed long distance behavior of the vortex-removed potential, we have been able to remove a source of contamination in the untouched potential fits and provide improved values for the fitted string tension for the first time.

For a given Ansatz, the fitted value of ρ on the two dynamical lattices are similar and are roughly double the fit value on the pure gauge ensemble. This indicates that the effects contributing to the medium to long-range behavior of the vortex-removed potential are mainly sensitive to the presence or absence of dynamical fermions, but are only weakly dependent on the sea quark mass.

There are indications of increased screening by the light dynamical fermions in both the untouched and vortex-only results. Significantly, at longer distances we observe both modified Ansätze show a decrease in the fitted value of the untouched and vortex-only string tensions when transitioning from the heavy to light pion mass.

As we have not corrected for short-distance lattice artifacts the fitted values of α should be interpreted with some caution, but are also worth discussing. The Coulomb term coefficients arising from the fits to the untouched potentials are summarized in Table VII (recalling that for the $V_{\rm as}$ Ansatz the effective short-distance coupling is $\tilde{\alpha}=\alpha/\rho$). For the pure gauge ensemble, the fitted values are close to the universal value of $\pi/12\simeq 0.26$ derived from a thin flux tube effective field theory [61]. We observe the Coulomb couplings increase with decreasing sea quark mass for all three Ansätze considered herein. This trend, which is indicative of dynamical fermion screening, has been previously observed for the standard potential fits [62]. It is interesting to see that this trend is replicated in our modified fits as well, as it suggests that the modified Coulomb terms are sensitive to the same short-distance physics as the standard Ansatz.

The crucial finding of this work is that the introduction of dynamical fermions at any pion mass induces a measurable shift in the behavior of center vortices. Applying the modified Ansätze introduced herein, the pure gauge vortex-only potential remains unable to reproduce the untouched string tension, whereas in contrast the respective dynamical string tensions show good agreement. The vortex-removed ensembles consistently show complete removal of the long range confining potential. This reinforces the argument that the salient nonperturbative properties of the ground state vacuum fields are encapsulated in the center vortex degrees of freedom.

TABLE VI. Ratios of the vortex-only to untouched string tensions from the Cornell and modified fit functions.

m_π(MeV)	$\sigma_{\rm VO}/\sigma_{\rm UT}^{\rm cornell}$	$\sigma_{\rm VO}/\sigma_{\rm UT}^{\rm as}$	$\sigma_{\rm VO}/\sigma_{\rm UT}^{\rm sc}$
Pure gauge	0.62(2)	0.60(2)	0.60(2)
701	1.06(2)	0.97(2)	0.97(2)
156	1.25(3)	1.05(2)	1.06(2)

TABLE VII. The (effective) Coulomb term coefficients from the Cornell and modified fits to the untouched potentials.

m_π(MeV)	$\alpha_{\rm UT}^{\rm cornell}$	$\tilde{\alpha}_{\rm UT}^{\rm as}$	$\alpha_{\rm UT}^{\rm sc}$
Pure gauge	0.286(7)	0.293(7)	0.301(7)
701	0.42(1)	0.49(2)	0.54(2)
156	0.61(4)	0.72(6)	0.84(7)

VI. CONCLUSION

In this work we have presented the first calculation of the static quark potential from center vortices obtained in the presence of dynamical fermions in QCD. The difficulties in fitting a standard Coulomb term to a wide range of vortex-removed values revealed a source of systematic contamination at moderate to large separations, resulting in the under estimation of the untouched string tension. In response we proposed two modified Coulomb Ansätze. The first modified Ansatz seeks to model the effect of antiscreening in the running coupling for QCD. The second modified Ansatz takes the form of a Yukawa potential, accommodating a dynamical effective gluon mass. Both Ansätze for the vortex-removed potential approach a constant value in the large r limit and are able to describe the static quark potential on the vortex-removed ensembles. Extending the modified Coloumb potentials with a linear string tension enables fits to the untouched potential.

The vortex-removed ensembles lack a linear confining potential for both the large and small pion masses considered here. Resolving the long-range behavior of the vortex-removed static quark potential with the fit parameter ρ enables us to remove a source of systematic contamination in the untouched potential fits, providing an improved determination of the untouched string tension. In doing so, we find good agreement between the vortex-only and untouched string tensions in the presence of dynamical fermions. The fact both modified Ansätze yield fit values for the string tension that are essentially identical suggests that any systematic errors introduced by the modifications are minimal. Evidence of quark loop screening is seen at the light quark mass.

These results suggest that the presence of dynamical fermions resolves the pure-gauge discrepancy between the original and vortex-only potential at large distances, presenting an important step in understanding the QCD vacuum. Historically, despite remarkable qualitative results, the center-vortex model has not agreed quantitatively with pure Yang-Mills calculations. It is fascinating to see that with the improvements presented here that good agreement is achieved for the string tension with the introduction of dynamical fermions in full QCD.

The mechanism for the observed phenomenological improvement is currently unknown. In pure gauge theory the identified center vortex string tension is dependent on the specific gauge fixing procedure [5,9,11,63,64]. For example, in Laplacian center gauge the full string tension is recovered [65–70]. Future investigations will revisit these gauge fixing dependencies with vortices derived from dynamical gauge fields in order to further understand the differences that have been observed herein.

Another avenue of improvement would be to expand the variational operator basis. In particular, the inclusion of a heavy-light meson-meson operator may clarify the long-range behavior of the vortex-modified potential and reveal possible connections to string breaking. We note that in the presence of dynamical fermions, string breaking implies that the static quark potential no longer rises indefinitely and as such we must reconsider precisely what is meant by quark confinement in this context.

The concept of *separation-of-charge* (S_c) confinement has been proposed elsewhere and studied in the context of the gauge-Higgs model [71–74]. Key to this concept is the existence of an order parameter, analogous to the Edwards-Anderson order parameter for spin-glass systems, that can be calculated to determine if a given vacuum phase is S_c-confining. It has not yet been verified numerically if QCD is S_c-confining. Testing the response of the corresponding order parameter to vortex projection/removal would be an interesting line of future study.

The relationship between dynamical fermions and the geometry of center vortices is also of interest, as it is well understood that the confining potential of center vortices arises from an area-law percolating behavior [5,25,75]. A direct examination of center-vortex structure complemented by probing of further quantities will assist in shedding light on the complex relationship between center vortices and the structure of the QCD vacuum.

Our findings strengthen the evidence that center vortices are responsible for the long-range confining potential of QCD and provide a first glimpse of the interplay between center vortices and dynamical fermions. Research to further explore center vortices in full QCD will be the subject of upcoming work.

ACKNOWLEDGMENTS

We thank the PACS-CS Collaboration for making their $2+1$ flavor configurations available via the International Lattice Data Grid (ILDG). This research was undertaken with the assistance of resources from the National Computational Infrastructure (NCI), provided through the National Computational Merit Allocation Scheme and supported by the Australian Government through Grant No. LE190100021 via the University of Adelaide Partner Share. This research is supported by Australian Research Council through Grants No. DP190102215 and No. DP210103706. W. K. is supported by the Pawsey Supercomputing Centre through the Pawsey Centre for Extreme Scale Readiness (PaCER) program. W. K. would like to thank Ross Young and Peter Tandy for valuable discussions. J. B. thanks Adam Virgili for helpful discussions on the smearing of vortex-only configurations.

[1] G. 't Hooft, On the phase transition towards permanent quark confinement, Nucl. Phys. **B138**, 1 (1978).
[2] G. 't Hooft, A property of electric and magnetic flux in non-Abelian gauge theories, Nucl. Phys. **B153**, 141 (1979).
[3] L. Del Debbio, M. Faber, J. Greensite, and S. Olejnik, Center dominance and Z(2) vortices in SU(2) lattice gauge theory, Phys. Rev. D **55**, 2298 (1997).
[4] M. Faber, J. Greensite, and S. Olejnik, Casimir scaling from center vortices: Towards an understanding of the adjoint string tension, Phys. Rev. D **57**, 2603 (1998).
[5] L. Del Debbio, M. Faber, J. Giedt, J. Greensite, and S. Olejnik, Detection of center vortices in the lattice Yang-Mills vacuum, Phys. Rev. D **58**, 094501 (1998).
[6] R. Bertle, M. Faber, J. Greensite, and S. Olejnik, The structure of projected center vortices in lattice gauge theory, J. High Energy Phys. 03 (1999) 019.
[7] M. Faber, J. Greensite, S. Olejnik, and D. Yamada, The vortex finding property of maximal center (and other) gauges, J. High Energy Phys. 12 (1999) 012.
[8] M. Engelhardt, K. Langfeld, H. Reinhardt, and O. Tennert, Deconfinement in SU(2) Yang-Mills theory as a center vortex percolation transition, Phys. Rev. D **61**, 054504 (2000).
[9] M. Engelhardt and H. Reinhardt, Center projection vortices in continuum Yang-Mills theory, Nucl. Phys. **B567**, 249 (2000).
[10] M. Engelhardt, Center vortex model for the infrared sector of Yang-Mills theory: Topological susceptibility, Nucl. Phys. **B585**, 614 (2000).
[11] R. Bertle, M. Faber, J. Greensite, and S. Olejnik, P vortices, gauge copies, and lattice size, J. High Energy Phys. 10 (2000) 007.
[12] K. Langfeld, H. Reinhardt, and J. Gattnar, Gluon propagators and quark confinement, Nucl. Phys. **B621**, 131 (2002).
[13] J. Greensite, The confinement problem in lattice gauge theory, Prog. Part. Nucl. Phys. **51**, 1 (2003).
[14] F. Bruckmann and M. Engelhardt, Writhe of center vortices and topological charge: An explicit example, Phys. Rev. D **68**, 105011 (2003).
[15] M. Engelhardt, M. Quandt, and H. Reinhardt, Center vortex model for the infrared sector of SU(3) Yang-Mills theory: Confinement and deconfinement, Nucl. Phys. **B685**, 227 (2004).
[16] P. Y. Boyko, V. G. Bornyakov, E. M. Ilgenfritz, A. V. Kovalenko, B. V. Martemyanov, M. Muller-Preussker, M. I. Polikarpov, and A. I. Veselov, Once more on the interrelation between Abelian monopoles and P-vortices in SU(2) LGT, Nucl. Phys. **B756**, 71 (2006).
[17] E.-M. Ilgenfritz, K. Koller, Y. Koma, G. Schierholz, T. Streuer, V. Weinberg, and M. Quandt, Localization of overlap modes and topological charge, vortices and monopoles in SU(3) LGT, *Proc. Sci.*, LATTICE2007 (2007) 311 [arXiv:0710.2607].
[18] V. G. Bornyakov, E. M. Ilgenfritz, B. V. Martemyanov, S. M. Morozov, M. Muller-Preussker, and A. I. Veselov, Interrelation between monopoles, vortices, topological charge and chiral symmetry breaking: Analysis using overlap fermions for SU(2), Phys. Rev. D **77**, 074507 (2008).
[19] A. O'Cais, W. Kamleh, K. Langfeld, B. Lasscock, D. Leinweber, P. Moran, A. Sternbeck, and L. von Smekal, Preconditioning maximal center gauge with stout link smearing in SU(3), Phys. Rev. D **82**, 114512 (2010).
[20] M. Engelhardt, Center vortex model for the infrared sector of SU(3) Yang-Mills theory: Topological susceptibility, Phys. Rev. D **83**, 025015 (2011).
[21] P. O. Bowman, K. Langfeld, D. B. Leinweber, A. Sternbeck, L. von Smekal, and A. G. Williams, Role of center vortices in chiral symmetry breaking in SU(3) gauge theory, Phys. Rev. D **84**, 034501 (2011).
[22] E.-A. O'Malley, W. Kamleh, D. Leinweber, and P. Moran, SU(3) centre vortices underpin confinement and dynamical chiral symmetry breaking, Phys. Rev. D **86**, 054503 (2012).
[23] A. Trewartha, W. Kamleh, and D. Leinweber, Connection between center vortices and instantons through gauge-field smoothing, Phys. Rev. D **92**, 074507 (2015).
[24] A. Trewartha, W. Kamleh, and D. Leinweber, Evidence that centre vortices underpin dynamical chiral symmetry breaking in SU(3) gauge theory, Phys. Lett. B **747**, 373 (2015).
[25] J. Greensite, Confinement from center vortices: A review of old and new results, EPJ Web Conf. **137**, 01009 (2017).
[26] A. Trewartha, W. Kamleh, and D. B. Leinweber, Centre vortex removal restores chiral symmetry, J. Phys. G **44**, 125002 (2017).
[27] J. C. Biddle, W. Kamleh, and D. B. Leinweber, Gluon propagator on a center-vortex background, Phys. Rev. D **98**, 094504 (2018).
[28] F. Spengler, M. Quandt, and H. Reinhardt, Branching of center vortices in SU(3) lattice gauge theory, Phys. Rev. D **98**, 094508 (2018).
[29] K. Langfeld, Vortex structures in pure SU(3) lattice gauge theory, Phys. Rev. D **69**, 014503 (2004).
[30] R. Bertle, M. Faber, J. Greensite, and S. Olejnik, Center vortices and color confinement in lattice QCD, arXiv:hep-lat/0009017.
[31] J. C. Biddle, W. Kamleh, and D. B. Leinweber, Visualization of center vortex structure, Phys. Rev. D **102**, 034504 (2020).
[32] S. Aoki *et al.* (PACS-CS Collaboration), $2 + 1$ flavor lattice QCD toward the physical point, Phys. Rev. D **79**, 034503 (2009).
[33] Y. Iwasaki, Renormalization group analysis of lattice theories and improved lattice action. II. Four-dimensional non-Abelian SU(N) gauge model, arXiv:1111.7054.
[34] A. Montero, Study of SU(3) vortex—like configurations with a new maximal center gauge fixing method, Phys. Lett. B **467**, 106 (1999).
[35] M. Albanese *et al.* (APE Collaboration), Glueball masses and string tension in lattice QCD, Phys. Lett. B **192**, 163 (1987).
[36] W. Kamleh, D. B. Leinweber, and A. G. Williams, Hybrid Monte Carlo with fat link fermion actions, Phys. Rev. D **70**, 014502 (2004).
[37] A. Virgili, W. Kamleh, and D. Leinweber, Smoothing algorithms for projected center-vortex gauge fields, Phys. Rev. D **106**, 014505 (2022).
[38] P. J. Moran and D. B. Leinweber, Over-improved stout-link smearing, Phys. Rev. D **77**, 094501 (2008).

[39] M. Luscher and P. Weisz, Definition and general properties of the transfer matrix in continuum limit improved lattice gauge theories, Nucl. Phys. **B240**, 349 (1984).
[40] D. B. Leinweber, R. M. Woloshyn, and T. Draper, Electromagnetic structure of octet baryons, Phys. Rev. D **43**, 1659 (1991).
[41] M. S. Mahbub, A. O. Cais, W. Kamleh, B. G. Lasscock, D. B. Leinweber, and A. G. Williams, Isolating excited states of the nucleon in lattice QCD, Phys. Rev. D **80**, 054507 (2009).
[42] G. S. Bali, H. Neff, T. Duessel, T. Lippert, and K. Schilling (SESAM Collaboration), Observation of string breaking in QCD, Phys. Rev. D **71**, 114513 (2005).
[43] J. Bulava, B. Hörz, F. Knechtli, V. Koch, G. Moir, C. Morningstar, and M. Peardon, String breaking by light and strange quarks in QCD, Phys. Lett. B **793**, 493 (2019).
[44] S. Aoki *et al.* (*CP*-PACS Collaboration), Comparative study of full QCD hadron spectrum and static quark potential with improved actions, Phys. Rev. D **60**, 114508 (1999).
[45] C. Michael, The running coupling from lattice gauge theory, Phys. Lett. B **283**, 103 (1992).
[46] R. G. Edwards, U. M. Heller, and T. R. Klassen, Accurate scale determinations for the Wilson gauge action, Nucl. Phys. **B517**, 377 (1998).
[47] R. Sommer, A new way to set the energy scale in lattice gauge theories and its applications to the static force and alpha-s in SU(2) Yang-Mills theory, Nucl. Phys. **B411**, 839 (1994).
[48] T. R. Klassen, The (Lattice) QCD potential and coupling: How to accurately interpolate between multiloop QCD and the string picture, Phys. Rev. D **51**, 5130 (1995).
[49] A. Deur, S. J. Brodsky, and G. F. de Teramond, The QCD running coupling, Nucl. Phys. **90**, 1 (2016).
[50] S. P. Booth, D. S. Henty, A. Hulsebos, A. C. Irving, C. Michael, and P. W. Stephenson (UKQCD Collaboration), The running coupling from SU(3) lattice gauge theory, Phys. Lett. B **294**, 385 (1992).
[51] G. S. Bali and K. Schilling, Running coupling and the Lambda parameter from SU(3) lattice simulations, Phys. Rev. D **47**, 661 (1993).
[52] M. Luscher, R. Sommer, P. Weisz, and U. Wolff, A Precise determination of the running coupling in the SU(3) Yang-Mills theory, Nucl. Phys. **B413**, 481 (1994).
[53] T. Blum, L. Karkkainen, D. Toussaint, and S. A. Gottlieb, The beta function and equation of state for QCD with two flavors of quarks, Phys. Rev. D **51**, 5153 (1995).
[54] K. Hornbostel, G. P. Lepage, and C. Morningstar, Scale setting for alpha(s) beyond leading order, Phys. Rev. D **67**, 034023 (2003).
[55] A. Bazavov, N. Brambilla, X. G. Tormo, I, P. Petreczky, J. Soto, and A. Vairo, Determination of α_s from the QCD static energy: An update, Phys. Rev. D **90**, 074038 (2014); Erratum, Phys. Rev. D **101**, 119902 (2020).
[56] J. E. Mandula and M. Ogilvie, The gluon is massive: A lattice calculation of the gluon propagator in the Landau gauge, Phys. Lett. B **185**, 127 (1987).
[57] I. L. Bogolubsky, E. M. Ilgenfritz, M. Muller-Preussker, and A. Sternbeck, The Landau gauge gluon and ghost propagators in 4D SU(3) gluodynamics in large lattice volumes, Proc. Sci., LATTICE2007 (**2007**) 290 [arXiv:0710.1968].
[58] I. L. Bogolubsky, E. M. Ilgenfritz, M. Muller-Preussker, and A. Sternbeck, Lattice gluodynamics computation of Landau gauge Green's functions in the deep infrared, Phys. Lett. B **676**, 69 (2009).
[59] S. W. Li, P. Lowdon, O. Oliveira, and P. J. Silva, The generalised infrared structure of the gluon propagator, Phys. Lett. B **803**, 135329 (2020).
[60] J. Horak, F. Ihssen, J. Papavassiliou, J. M. Pawlowski, A. Weber, and C. Wetterich, Gluon condensates and effective gluon mass, arXiv:2201.09747.
[61] M. Luscher, Symmetry breaking aspects of the roughening transition in gauge theories, Nucl. Phys. **B180**, 317 (1981).
[62] G. S. Bali, B. Bolder, N. Eicker, T. Lippert, B. Orth, P. Ueberholz, K. Schilling, and T. Struckmann (TXL, T(X)L Collaborations), Static potentials and glueball masses from QCD simulations with Wilson sea quarks, Phys. Rev. D **62**, 054503 (2000).
[63] T. G. Kovacs and E. T. Tomboulis, On P vortices and the Gribov problem, Phys. Lett. B **463**, 104 (1999).
[64] M. Faber, J. Greensite, and S. Olejnik, Remarks on the Gribov problem in direct maximal center gauge, Phys. Rev. D **64**, 034511 (2001).
[65] J. C. Vink and U.-J. Wiese, Gauge fixing on the lattice without ambiguity, Phys. Lett. B **289**, 122 (1992).
[66] C. Alexandrou, M. D'Elia, and P. de Forcrand, The Relevance of center vortices, Nucl. Phys. B, Proc. Suppl. **83**, 437 (2000).
[67] P. de Forcrand and M. Pepe, Center vortices and monopoles without lattice Gribov copies, Nucl. Phys. **B598**, 557 (2001).
[68] M. Faber, J. Greensite, and S. Olejnik, Center dominance recovered: Direct Laplacian center gauge, Nucl. Phys. B, Proc. Suppl. **106**, 652 (2002).
[69] M. Faber, J. Greensite, and S. Olejnik, Direct Laplacian center gauge, J. High Energy Phys. 11 (2001) 053.
[70] K. Langfeld, H. Reinhardt, and A. Schafke, Center vortex properties in the Laplace center gauge of SU(2) Yang-Mills theory, Phys. Lett. B **504**, 338 (2001).
[71] J. Greensite and K. Matsuyama, Confinement criterion for gauge theories with matter fields, Phys. Rev. D **96**, 094510 (2017).
[72] J. Greensite and K. Matsuyama, What symmetry is actually broken in the Higgs phase of a gauge-Higgs theory?, Phys. Rev. D **98**, 074504 (2018).
[73] J. Greensite and K. Matsuyama, Higgs phase as a spin glass and the transition between varieties of confinement, Phys. Rev. D **101**, 054508 (2020).
[74] J. Greensite and K. Matsuyama, Symmetry, Confinement, and the Higgs Phase, Symmetry **14**, 177 (2022).
[75] H. G. Dosch and Yu. A. Simonov, The area law of the Wilson loop and vacuum field correlators, Phys. Lett. B **205**, 339 (1988).